



HAL
open science

Field-induced spin-density wave beyond hidden order in **URu₂Si₂**

William Knafo, F. Duc, Frederic Bourdarot, K. Kuwahara, H. Nojiri, D. Aoki,
Julien Billette, P. Frings, X. Tonon, E. Lelièvre-Berna, et al.

► **To cite this version:**

William Knafo, F. Duc, Frederic Bourdarot, K. Kuwahara, H. Nojiri, et al.. Field-induced spin-density wave beyond hidden order in URu₂Si₂. Nature Communications, 2016, 7 (1), pp.13075. 10.1038/ncomms13075 . hal-01943387

HAL Id: hal-01943387

<https://hal.science/hal-01943387v1>

Submitted on 12 Jun 2019

HAL is a multi-disciplinary open access archive for the deposit and dissemination of scientific research documents, whether they are published or not. The documents may come from teaching and research institutions in France or abroad, or from public or private research centers.

L'archive ouverte pluridisciplinaire **HAL**, est destinée au dépôt et à la diffusion de documents scientifiques de niveau recherche, publiés ou non, émanant des établissements d'enseignement et de recherche français ou étrangers, des laboratoires publics ou privés.

ARTICLE

Received 25 Mar 2016 | Accepted 31 Aug 2016 | Published 20 Oct 2016

DOI: 10.1038/ncomms13075

OPEN

Field-induced spin-density wave beyond hidden order in URu₂Si₂

W. Knafo¹, F. Duc¹, F. Bourdarot², K. Kuwahara³, H. Nojiri⁴, D. Aoki^{5,6}, J. Billette¹, P. Frings¹, X. Tonon⁷, E. Lelièvre-Berna⁷, J. Flouquet⁶ & L.-P. Regnault⁷

URu₂Si₂ is one of the most enigmatic strongly correlated electron systems and offers a fertile testing ground for new concepts in condensed matter science. In spite of >30 years of intense research, no consensus on the order parameter of its low-temperature hidden-order phase exists. A strong magnetic field transforms the hidden order into magnetically ordered phases, whose order parameter has also been defying experimental observation. Here, thanks to neutron diffraction under pulsed magnetic fields up to 40 T, we identify the field-induced phases of URu₂Si₂ as a spin-density-wave state. The transition to the spin-density wave represents a unique touchstone for understanding the hidden-order phase. An intimate relationship between this magnetic structure, the magnetic fluctuations and the Fermi surface is emphasized, calling for dedicated band-structure calculations.

¹Laboratoire National des Champs Magnétiques Intenses, UPR 3228, CNRS-UPS-INSA-UGA, 143 Avenue de Rangueil, 31400 Toulouse, France. ²Service de Modélisation et d'Exploration des Matériaux, Université Grenoble Alpes et Commissariat à l'Energie Atomique, INAC, 17 rue des Martyrs, 38054 Grenoble, France. ³Institute of Quantum Beam Science, Ibaraki University, Mito 310-8512, Japan. ⁴Institute for Materials Research, Tohoku University, Sendai 980-8578, Japan. ⁵Institute for Materials Research, Tohoku University, Ibaraki 311-1313, Japan. ⁶Service Photonique, Electronique et Ingénierie Quantiques, Université Grenoble Alpes et Commissariat à l'Energie Atomique, INAC, 17 rue des Martyrs, 38054 Grenoble, France. ⁷Institut Laue-Langevin, 71 Avenue des Martyrs, CS 20156, 38042 Grenoble, France. Correspondence and requests for materials should be addressed to W.K. (email: william.knafo@lncmi.cnrs.fr).

For since three decades, a huge experimental and theoretical effort has been employed to try to determine the ground state of the heavy-fermion material URu₂Si₂, where a second-order phase transition occurs at the temperature $T_0 = 17.5$ K and for which the order parameter has resisted experimental identification¹. The case of URu₂Si₂—which is also superconducting²—is not isolated, since mysterious electronic phases, identified as ‘pseudo-gap’ and ‘nematic’ phases, have also been reported in high-temperature cuprate and iron-based superconducting materials^{3,4}. Initially, a small magnetic moment of 0.02 Bohr magneton per uranium (μ_B/U) antiferromagnetically aligned along **c** and modulated with the wavevector $\mathbf{k}_0 = (0\ 0\ 1)$ has been considered as the order parameter of URu₂Si₂ below T_0 (ref. 5). However, this moment is too small to account for the large entropy associated with the transition and is now suspected to result from sample inhomogeneities⁶. In the hidden-order phase, the low-energy magnetic fluctuations are peaked at the hot wavevectors \mathbf{k}_0 and $\mathbf{k}_1 = (0.6\ 0\ 0)^{7,8}$, and the Fermi surface presents nesting with these two wavevectors^{9–15}, suggesting an itinerant origin of the magnetic properties. Recent experimental works have been interpreted as the signature of nematicity, that is, a correlated electronic state associated with a breaking of the fourfold symmetry, in the hidden-order phase^{16–18}.

The application of extreme conditions permits to modify the ground state of a system and get new insights about it. In URu₂Si₂ under pressure, the hidden-order state is replaced by an antiferromagnetic phase¹⁹, whose order parameter is a moment of $\approx 0.3–0.4\ \mu_B/U$ aligned antiferromagnetically along **c** with the wavevector \mathbf{k}_0 (refs 20,21). From the similar Fermi surfaces observed in the hidden-order and pressure-driven antiferromagnetic phases, it has been proposed that the hidden order, although of unknown nature, has a periodicity of wavevector \mathbf{k}_0 (ref. 19). Under a high magnetic field applied

along the easy magnetic axis **c**, a cascade of first-order phase transitions at the fields $\mu_0 H_1 = 35$ T, $\mu_0 H_2 = 36/37$ T (rising/falling fields), and $\mu_0 H_3 = 39$ T, leads to a polarized paramagnetic regime above H_3 , where a magnetization of $\approx 1.4\ \mu_B/U$ is reached (Fig. 1b)^{22,23}. Quantum oscillations probes have shown that a magnetic field along **c** induces Fermi surface instabilities deep inside the hidden-order phase, as well as at the magnetic transitions H_1 , H_2 and H_3 (refs 24–28). By comparison with 3d itinerant magnets, a novelty in heavy-fermion compounds is that a large magnetic polarization can be induced by a magnetic field, opening the path to new phases driven by combined changes of magnetic order and Fermi surface. Such interplay of metamagnetic and Lifshitz transitions has been evidenced in the heavy-fermion paramagnet CeRu₂Si₂ (ref. 29).

In Rh-doped U(Ru_{0.96}Rh_{0.04})₂Si₂, no hidden-order phase is reported, but first-order transitions are also induced at magnetic fields of 26 and 37 T applied along **c** (refs 30–32). Between 26 and 37 T, a squared up–up–down ferrimagnetic phase was deduced from Bragg peaks (harmonics) at the wavevector $\mathbf{k}_2 = (2/3\ 0\ 0)$ and at the Brillouin zone centre $\mathbf{k}_{ZC} = (0\ 0\ 0)^{33}$. However, the extrapolation to the pure case of URu₂Si₂ is not straightforward, as doping may modify the low-carrier content of the pure lattice, and, thus, the Fermi surface topology, leading to different nesting effects. Here thanks to a new cryomagnet allowing neutron diffraction up to 40 T, we have determined the magnetic structure of URu₂Si₂ in fields between 35 and 39 T. A tilt by 4.2° of the field direction from **c** in the (**c**,**a**) plane allowed accessing a large number of momentum transfers **Q**, with almost no modification of the magnetic phase diagram expected for **H** || **c** (refs 26,34). The relationship between the high-field magnetic structure, the low-energy magnetic fluctuations and the Fermi surface is emphasized, appealing for new band-structure calculations describing the electronic properties of URu₂Si₂.

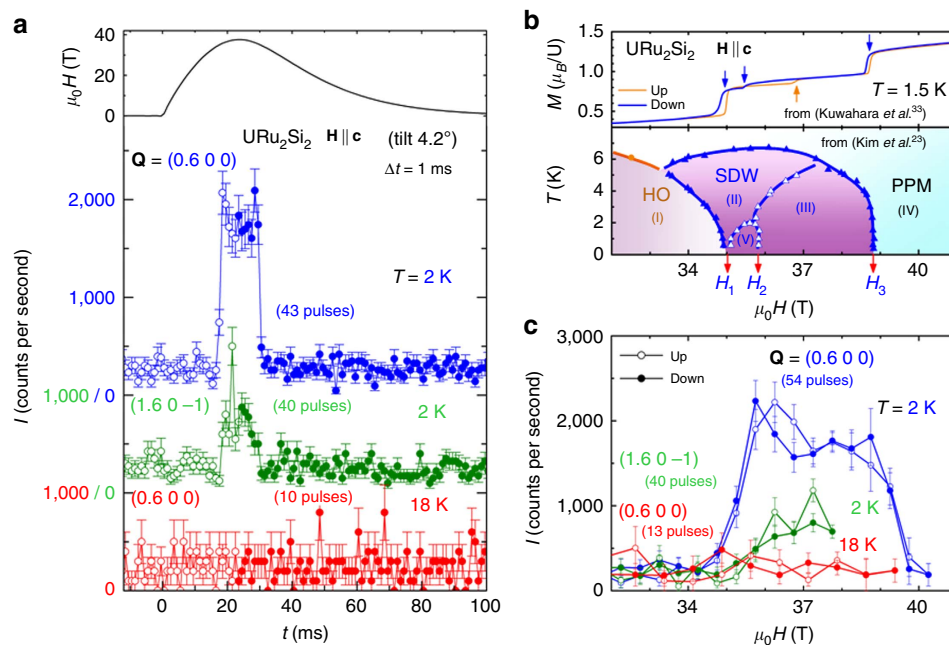


Figure 1 | Signatures of the field-induced magnetic phases. (a) Time profile of a field pulsed up to 38 T, and time dependence of the diffracted intensity at $\mathbf{Q} = (0.6\ 0\ 0)$ and $T = 2$ K, $\mathbf{Q} = (1.6\ 0\ -1)$ and $T = 2$ K, and $\mathbf{Q} = (0.6\ 0\ 0)$ and $T = 18$ K, in fields up to 38 T, integrated within time steps $\Delta t = 1$ ms. The error bars ΔI are given by the square root of the neutron counts ($\Delta I = \sqrt{I/\tau}$, where τ is the total accumulation time over several pulses). (b) Magnetization versus magnetic field at $T = 1.5$ K (from ref. 33) and magnetic field-temperature phase diagram deduced from magnetoresistivity versus temperature and versus field, in falling fields (from ref. 23). (c) Field dependence of the same diffracted intensities in fields up to 40.5 T, integrated within field steps $\Delta(\mu_0 H) = 0.5$ T. Open and full symbols correspond to rising and falling fields, respectively. The magnetic field has been applied along the easy magnetic axis **c** with a tilt of 4.2° along **a**.

Results

Spin-density wave with wavevector \mathbf{k}_1 . Figure 1a shows the time profile of a magnetic field pulsed up to 38 T, as well as the time dependence of the diffracted neutron intensities recorded during 38-T pulses at the temperatures $T=2$ and 18 K and at $\mathbf{Q}=(0.6\ 0\ 0)$ and $(1.6\ 0\ -1)$. These momentum transfers are satellites of wavevector $\mathbf{k}_1=(0.6\ 0\ 0)=\mathbf{Q}-\boldsymbol{\tau}$ around the structural Bragg positions $\boldsymbol{\tau}=(0\ 0\ 0)$ and $(1\ 0\ -1)$, respectively. The high-field enhancement of the diffracted intensity at $T=2$ K, absent at $T=18$ K, shows that long-range ordering with wavevector $\mathbf{k}_1=(0.6\ 0\ 0)$ is established at high field and low temperature. Figure 1c emphasizes in the window 32–41 T the field dependence of the diffracted neutron intensities measured up to 40.5 T. At $T=2$ K, the diffracted intensity with wavevector \mathbf{k}_1 is enhanced in fields higher than $\mu_0H_1=35$ T and drops down to the background level in fields higher than $\mu_0H_3=39$ T. No hysteresis is observed at H_1 and H_3 within the neutron counting statistics, and a slight field-induced decrease of intensity, suggesting a modification of magnetic ordering, is visible at $\mu_0H_2\approx 36$ T for rising field and at $\mu_0H_2\approx 37$ T for falling field, in agreement with the hysteresis observed by magnetization³³ (Fig. 1b). Figure 2 presents the high-field neutron-diffracted intensity at momentum transfers \mathbf{Q} in the vicinity of $(0.6\ 0\ 0)$ at $T=2$ K. The field dependence of the intensity at momentum transfers $(Q_h\ 0\ 0)$ and $(0.6\ 0\ Q_z)$ is shown in fields up to 36.2 T in Fig. 2a,b, respectively. Figure 2c,d presents Q_h - and Q_z -scans at $\mu_0H=36$ T, confirming that the field-induced magnetic intensity is peaked at $\mathbf{Q}=(0.6\ 0\ 0)$. From the intensity of the magnetic Bragg peaks induced at $\mathbf{Q}=(0.6\ 0\ 0)$ and $\mathbf{Q}=(1.6\ 0\ -1)$ at $\mu_0H=36\text{ T} > \mu_0H_1$, we extract the amplitude $2M(\mathbf{k}_1)\approx 0.5 \pm 0.05\ \mu_B/U$ of the sine modulation with wavevector \mathbf{k}_1 of the magnetic moment $M(\mathbf{k}_1, \mathbf{r})=2M(\mathbf{k}_1)\cos(2\pi\mathbf{k}_1\cdot\mathbf{r}+\varphi_1)$, where \mathbf{r} is an U-ion position and φ_1 the associated phase (cf. Supplementary Note 1). This result is in agreement with the high-field magnetization²², since the amplitude $2M(\mathbf{k}_1)$ extracted here at 36 T is of same order than the variation of magnetization $\Delta M\approx 0.4\ \mu_B/U$ (estimated from 36–39 T) induced by the quench of the field-induced ordered moments into a polarized regime above $\mu_0H_3=39$ T.

The field dependence of the diffracted intensity is presented in Fig. 3 for a large set of momentum transfers \mathbf{Q} from $(Q_h\ 0\ 0)$, $(Q_h\ 0\ -1)$ and $(1\ 0\ Q_z)$ scans in the reciprocal space at $T=2$ K. Except at $\mathbf{Q}=(0.6\ 0\ 0)$ and $(1.6\ 0\ -1)$ corresponding to \mathbf{k}_1 , no field-induced change of the neutron-diffracted intensity is observed at the different probed momentum transfers. In particular, no change of intensity occurs in high field at the harmonics $n\mathbf{k}_1$, where $n\neq 1$ is an integer, including the Brillouin zone centre $\mathbf{k}_{ZC}=(0\ 0\ 0)$, within an error of ~ 5 –10% of the induced intensity at \mathbf{k}_1 (cf. Supplementary Table 1). The absence of harmonics supports that the high-field magnetic structure is a spin-density wave, that is, a sine-modulated magnetic structure, in opposition with a squared-modulated structure, where harmonics of the main wavevector would lead to full moments, either up or down, on the U sites (cf. Supplementary Note 2). Spin-density-wave modulations of the magnetic moment are generally observed at low temperature in itinerant magnets at zero field, as chromium³⁵, or, in a magnetic field, as the heavy-fermion superconductor CeCoIn₅ (ref. 36) and the low-dimensional magnet Sr₃Ru₂O₇ (ref. 37). However, in the present case, we cannot fully exclude the possibility of a ‘special’ sequence of squared Ising moments, for which high-order harmonics $n\mathbf{k}_1$ would all have intensities smaller than our error bar, that is, 5–10% of the magnetic intensity at \mathbf{k}_1 . The absence of neutron Bragg peaks at $\mathbf{k}_2=(2/3\ 0\ 0)$ and \mathbf{k}_{ZC} is in contradiction with the up–up–down squared modulation proposed from nuclear magnetic resonance (NMR) measured on URu₂Si₂ in

the field window 35.5–36.5 T (ref. 38). The NMR spectrum, composed of a central narrow peak and two broad satellites, is not compatible with a single- \mathbf{k} spin-density wave, which would lead either to a few discrete and thin peaks (if \mathbf{k}_1 is commensurate) or to a double-horn line shape (if \mathbf{k}_1 is incommensurate)³⁸. However, an incommensurability of \mathbf{k}_1 (that is, a slight deviation from $(0.6\ 0\ 0)$ compatible with our neutron resolution $\Delta\mathbf{k}\approx(\pm 0.01\ \pm 0.05\ \pm 0.003)$), combined with a multi- \mathbf{k} character of the spin-density wave, could induce peculiar features, as a central peak, in the NMR spectrum³⁹, and could possibly reconcile the NMR and neutron studies. Such multi- \mathbf{k} structure would imply a conservation of the fourfold symmetry, that is, of the equivalence between x and y , in the high-field spin-density-wave phase, in contrast with the twofold symmetry proposed in refs 16,17 for the low-field hidden-order phase.

Absence of a ferromagnetic Bragg peak. Surprisingly, the neutron-diffracted intensity at the Brillouin zone centre \mathbf{k}_{ZC} is field invariant, while the magnetization M is strongly enhanced above 35 T (ref. 22). Usually, a magnetic Bragg peak develops at \mathbf{k}_{ZC} and has an intensity $\propto M^2$. From $M\approx 0.5$ – $1\ \mu_B/U$ in the field window 35–39 T, and assuming a magnetic form factor corresponding to localized f electrons (estimated from a low-field study of the magnetic form factor⁴⁰), one expects a magnetic intensity of $\approx 2,000$ – $8,000$ counts per s, in addition to the non-magnetic Bragg peak of $\approx 19,000$ counts per s, at $\mathbf{Q}=(1\ 0\ -1)$ corresponding to \mathbf{k}_{ZC} (cf. Supplementary Note 1). However, no such change of intensity is observed here at $\mathbf{Q}=(1\ 0\ -1)$, within an error of 200 counts per s. Several scenarios could explain this unexpected feature. (i) The absence of a magnetic Bragg peak at \mathbf{k}_{ZC} could result from a strongly-reduced magnetic form factor f_M related to itinerant electrons. Since the observation of magnetic Bragg peaks at $\mathbf{Q}=(0.6\ 0\ 0)$ and $(1.6\ 0\ -1)$ demonstrates that nearly localized electrons with $f_M\lesssim 1$ drive the high-field spin-density wave of wavevector \mathbf{k}_1 , scenario (i) would imply that the high-field magnetism would be localized, or nearly localized, at \mathbf{k}_1 but itinerant at \mathbf{k}_{ZC} . (ii) Alternatively, the absence of magnetic Bragg peak at \mathbf{k}_{ZC} could be explained by field-induced magnetic excitations at \mathbf{k}_{ZC} , which would contribute to the enhanced magnetization (cf. Kramers–Kronig relationship⁴¹), but not to the magnetic Bragg peak at \mathbf{k}_{ZC} . (iii) Finally, this absence could also result from a high-field decrease of the nuclear Bragg peak at $\mathbf{Q}=(1\ 0\ -1)$ (related via local stress effects to a change of some atomic positions), which would counteract the increase of magnetic intensity at \mathbf{k}_{ZC} . The missing magnetic Bragg intensity at \mathbf{k}_{ZC} constitutes an open question and will merit further studies.

Relationship with Fermi surface nesting. In an itinerant picture of magnetism, long-range magnetic ordering with a wavevector \mathbf{k}_m can be related to a partial or complete nesting of two parts of the Fermi surface. The dual localized itinerant behaviour is a central issue in heavy-fermion metals, where the magnetic properties often result from itinerant f electrons. In URu₂Si₂, 5 f electrons hybridize with electrons from the conduction bands and modifications of the Fermi surface and carrier mobility accompany the establishment of the hidden-order phase at the temperature T_0 (refs 26,42–45). The itinerancy of the f electrons has already been shown to be a key ingredient for the magnetic properties of this system. Angle-resolved photoemission spectroscopy and band-structure calculations showed that Fermi surfaces centred on the Γ and Z points are nested with the wavevector \mathbf{k}_0 (refs 9–12,15). In refs 9,15, a nesting with the wavevector \mathbf{k}_1 between Fermi surface ‘petals’ around the Γ point has been identified. In refs 11,12, a nesting with the wavevector

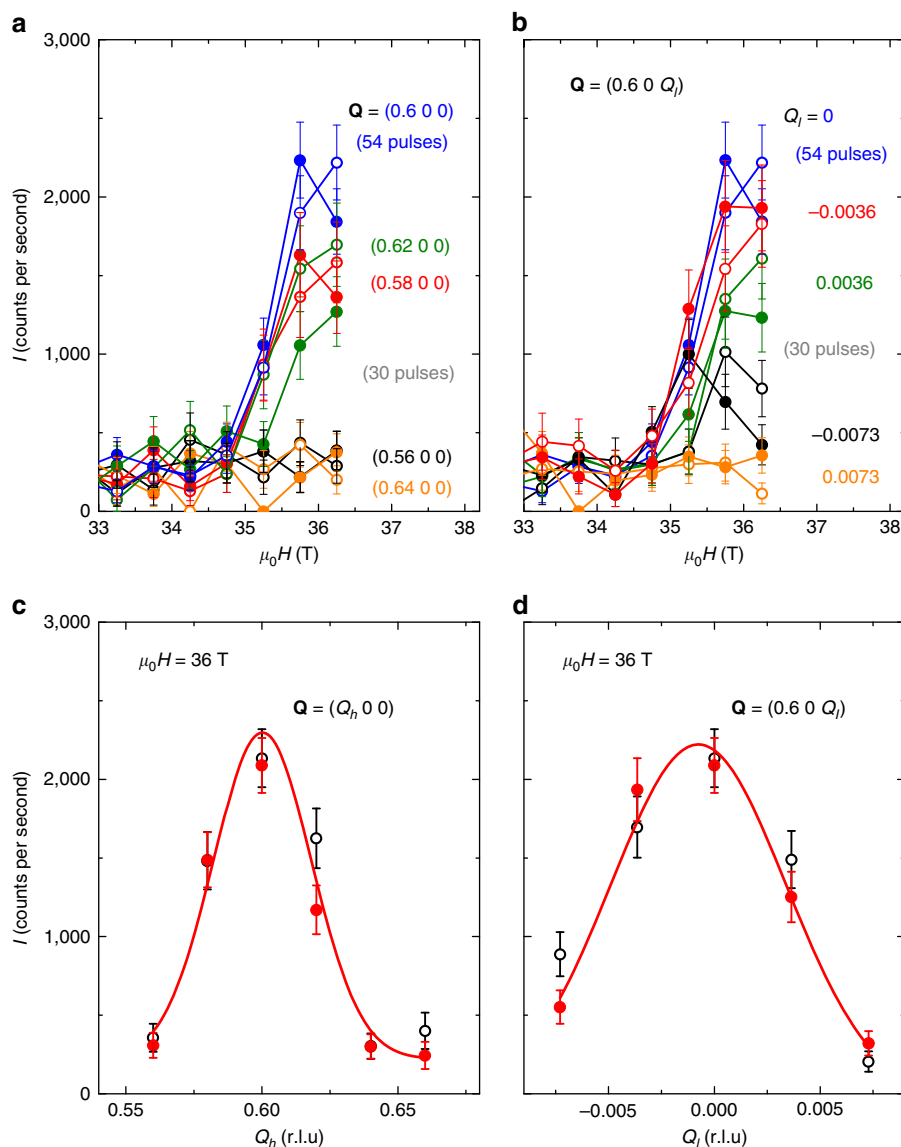


Figure 2 | High-field neutron diffraction at momentum transfers close to Q_1 , at $T = 2$ K. Magnetic field dependence of the neutron-diffracted intensity (a) at momentum transfers $\mathbf{Q} = (Q_h 0 0)$ and (b) at momentum transfers $\mathbf{Q} = (0.6 0 Q_l)$, in fields up to 36.2 T, within field steps $\Delta(\mu_0 H)$ of 0.5 T. (c) Q_h and (d) Q_l scans around the momentum transfer $\mathbf{Q}_1 = (0.6 0 0)$ under a magnetic field $\mu_0 H = 36$ T (field window $\Delta(\mu_0 H) = 1$ T). The error bars ΔI are given by the square root of the neutron counts ($\Delta I = \sqrt{I/\tau}$). Open and full symbols correspond to rising and falling fields, respectively. The magnetic field \mathbf{H} has been applied along the easy magnetic axis \mathbf{c} with a tilt of 4.2° along \mathbf{a} .

(0.4 0 0) between these petals and a Fermi surface centred on the Γ point has also been found. In ref. 14, another picture has been proposed, with a nesting with wavevector \mathbf{k}_0 between small Fermi pockets centred on the X points (defined in the first Brillouin zone) and a nesting with wavevector \mathbf{k}_1 between Fermi surfaces centred on the Γ and Z points. Despite these nesting of the Fermi surface, no long-range magnetic order has been reported yet in URu_2Si_2 in its hidden-order phase. Instead of long-range magnetic order, inelastic magnetic excitations at the wavevectors \mathbf{k}_0 and \mathbf{k}_1 have been observed by neutron scattering in the hidden-order phase^{5–8}. Their relationship with nesting effects and long-range magnetic ordering will be discussed below.

Assuming a high-rank multipolar order with wavevector \mathbf{k}_0 , which cannot be seen directly by neutron diffraction, band-structure calculations resulted in a Fermi surface of the hidden-order state, which is very similar to that of the pressure-induced antiferromagnetic state⁹, in accordance with the experimental observations¹⁹. Under a high magnetic field

applied along \mathbf{c} , successive Fermi surface modifications occur inside the hidden-order phase and at the transition fields H_1 , H_2 and H_3 delimiting the high-field phases^{24–28}. Several Fermi surface instabilities in fields smaller than $\mu_0 H_1 = 35$ T, that is, inside the hidden-order phase^{24,26–28}, are due to Lifshitz transitions and suggest a progressive modification of Fermi surface nestings. Resulting from the Fermi surface reconstruction at H_1 , the Fermi surface nesting with \mathbf{k}_1 is probably reinforced, leading to the onset of the spin-density wave observed here with the wavevector \mathbf{k}_1 .

Magnetic fluctuations as a precursor of magnetic ordering.

Figure 4 presents the magnetic phase diagram of URu_2Si_2 under pressure and magnetic field, over a wide range of temperatures up to 75 K. At zero field and ambient pressure, URu_2Si_2 is in a correlated paramagnetic regime below $T_{\chi}^{\text{max}} = 55$ K at which the static magnetic susceptibility χ is maximal²². The correlations are

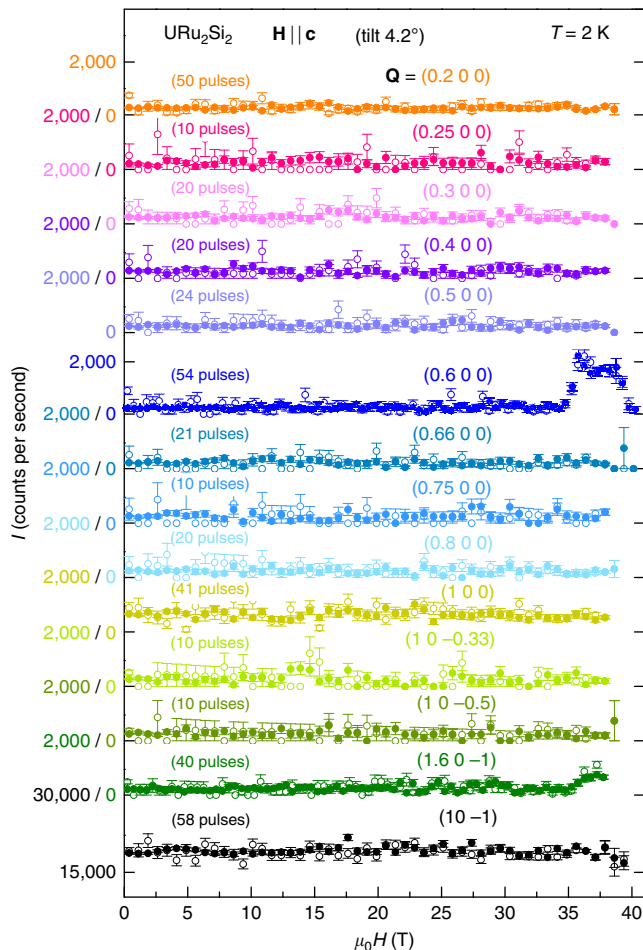


Figure 3 | Neutron-diffracted intensity for a large set of momentum transfers. Magnetic fields were applied up to 40.5 T, at a temperature $T = 2$ K. The error bars ΔI are given by the square root of the neutron counts ($\Delta I = \sqrt{I/\tau}$). Open and full symbols correspond to rising and falling fields, respectively. The magnetic field \mathbf{H} has been applied along the easy magnetic axis \mathbf{c} with a tilt of 4.2° along \mathbf{a} .

accompanied by a strong and broad magnetic-fluctuation spectrum peaked at the wavevector \mathbf{k}_1 , which progressively sets at temperatures of the order of T_χ^{\max} (ref. 8). When the system enters in its hidden-order phase, the magnetic fluctuations give rise to sharp inelastic spectra at the wavevectors \mathbf{k}_0 and \mathbf{k}_1 , with the gaps $\Delta E_0 \simeq 1.7$ meV and $\Delta E_1 \simeq 4.5$ meV, respectively, at low temperature. Below T_0 , the intensity of the magnetic fluctuations at \mathbf{k}_0 suddenly develops, while the intensity of the fluctuations at \mathbf{k}_1 , as indicated by the static susceptibility $\chi'(\mathbf{k}_1, E = 0)$, drops by 20% (refs 8,46).

The magnetic fluctuations peaked at the hot wavevectors \mathbf{k}_0 and \mathbf{k}_1 indicate the proximity of quantum-phase transitions associated with long-range ordering with the same wavevectors. Such precursory role of the magnetic fluctuations has been emphasized in the heavy-fermion paramagnet CeRu_2Si_2 , where doping (La, Rh or Ge) and magnetic field permit to tune competing quantum instabilities (cf. ref. 47 and refs therein). With pressure^{20,21} (as well as Rh doping³⁰), URu_2Si_2 can be tuned to antiferromagnetic long-range order with wavevector \mathbf{k}_0 . The disappearance of the hidden order in URu_2Si_2 under pressure coincides with a transfer of weight from magnetic fluctuations with wavevector \mathbf{k}_0 into antiferromagnetic order with the same wavevector^{48,49}. Contrary to those with \mathbf{k}_0 , the fluctuations with wavevector \mathbf{k}_1 survive under pressure⁴⁸ and their progressive

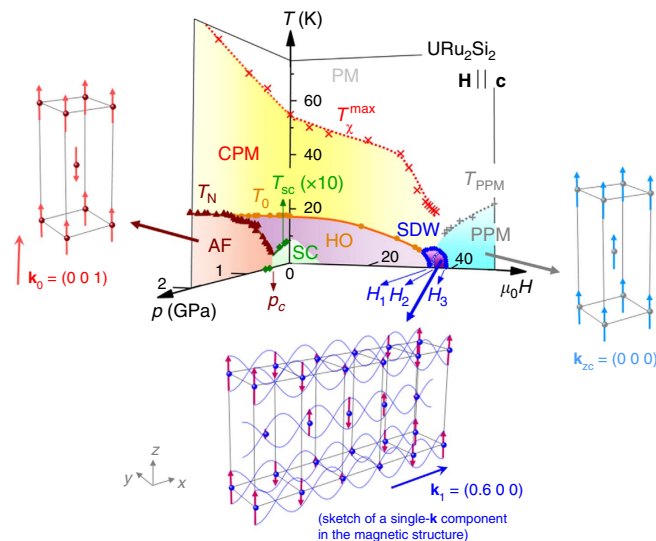


Figure 4 | Temperature-magnetic field and temperature-pressure phase diagrams of URu_2Si_2 . PM, CPM and PPM are the high-temperature, the low-temperature correlated and the high-field polarized paramagnetic regimes, respectively, HO and SC the hidden-order and superconducting phases, respectively, AF the antiferromagnetic state, and SDW the spin-density-wave state. For the AF, SDW and PPM regimes, a sketch of the magnetic structure is shown, where the spheres correspond to the U ions and the arrows represent their magnetic moments. For clarity, a single-component (wavevector $\mathbf{k}_1 = (0.6\ 0\ 0)$) sine modulation is shown for the SDW, which is suspected to be multi- \mathbf{k} . Data points in the phase diagram have been compiled from refs 19,22,23,31,50.

variation may be in relationship with the continuous evolution of T_χ^{\max} (ref. 50). With magnetic field, a spin-density wave is stabilized with the wavevector \mathbf{k}_1 . Both T_χ^{\max} and T_0 vanish in the quantum critical area $\mu_0 H \simeq 35\text{--}39$ T (ref. 22) where long-range magnetic ordering sets in. In the polarized regime above $\mu_0 H_3 = 39$ T, from the magnetization $> 1.4 \mu_B/\text{U}$, one can expect a loss of intersite magnetic correlations at \mathbf{k}_0 and \mathbf{k}_1 , the magnetic excitations becoming wavevector-independent, that is, of local nature. This picture is compatible with the observation in fields up to 17 T that the gap in the excitations at \mathbf{k}_0 increases with H , while that in the excitations at \mathbf{k}_1 remains constant, their extrapolations converging at $\simeq 35$ T (ref. 51). In the critical field window (35 and 39 T), the enhancement of the Sommerfeld coefficient²² is the signature of critical fluctuations, presumably of magnetic origin (cf. CeRu_2Si_2 , where critical magnetic fluctuations were reported at the La-doping- and magnetic-field-induced instabilities^{52,53}). However, inelastic neutron scattering under steady fields up to 40 T, which is far beyond the present state of the art (26 T achieved recently at the neutron source in Berlin⁵⁴), would be needed to unveil the high-field evolution of the magnetic fluctuations in URu_2Si_2 .

Discussion

We succeeded in detecting a high-magnetic-field switch from hidden-order to spin-density-wave phases in URu_2Si_2 . This result illustrates the dual localized and itinerant facets of the 5f electrons in this system. The relationship between Fermi surface nesting and the magnetic wavevector \mathbf{k}_1 of the spin-density wave, as well as the cascade of Lifshitz transitions induced by the high-field magnetic polarization^{24–28}, show the itinerant character of the 5f electrons. The neutron-diffracted intensity with the wavevector \mathbf{k}_1 is compatible with the magnetic form factor f_M corresponding to U^{3+} or U^{4+} configurations⁴⁰ and highlights the localized

character of the 5f electrons. Knowing that a change of the Fermi surface in the polarized regime of URu₂Si₂ was detected indirectly by Hall effect⁵⁵ and directly by quantum oscillations experiments²⁵, a challenge is to determine whether the missing magnetic Bragg peak at the wavevector $\mathbf{k}_{ZC} = (0\ 0\ 0)$ in a high magnetic field could be related to a change in the itinerancy of the f-electrons.

A relationship between the long-range magnetic order, the Fermi surface and the magnetic fluctuations has been highlighted. In the hidden-order phase, one may suspect ‘inelastic’ nestings between electronic band surfaces of different energies, to be connected with the observed gapped magnetic excitations at the wavevectors \mathbf{k}_0 and \mathbf{k}_1 (refs 5–8). These excitations are precursors of the long-range ordered states induced under magnetic field and pressure. Under a magnetic field, the transformation of the paramagnetic state with gapped magnetic excitations into a spin-density wave with wavevector \mathbf{k}_1 might be related to the stabilization of Fermi surface nesting with the wavevector \mathbf{k}_1 . Under pressure, a modification of the Fermi surface nesting with the wavevector \mathbf{k}_0 might also lead to long-range magnetic order with the wavevector \mathbf{k}_0 . Additional effects, as modifications of the crystal field, could also play a role in the stabilization of magnetically ordered phases.

Interestingly, the effect of Rh doping leads to a decrease of T_0 and T_Z^{max} (refs 30,31) similar to the magnetic field effect, and to antiferromagnetic order with wavevector \mathbf{k}_0 (for Rh contents $0.02 \leq x \leq 0.03$) similar to the pressure effect. The main wavevector $\mathbf{k}_2 = (2/3\ 0\ 0)$ of the high-field squared magnetic structure of U(Ru_{0.96}Rh_{0.04})₂Si₂ (ref. 33) is rather close to the wavevector $\mathbf{k}_1 = (0.6\ 0\ 0)$ of the spin-density wave of URu₂Si₂, confirming a relationship between these two magnetic phases. The differences between these wavevectors might result from subtle differences in the band structures of the two compounds, due to the doping sensibility of their low-carrier density.

Our observation of a spin-density wave in magnetic fields between 35 and 39 T will certainly push to develop models incorporating on equal basis the Fermi surface topology and the magnetic interactions. With the objective to describe competing quantum-phase transitions between the hidden-order and long-range ordered phases, such models will be a basis to solve the hidden-order problem. From an instrumental point of view, this work paves the way for neutron magnetic diffraction on weak-moment systems under pulsed magnetic field up to 40 T.

Methods

Samples. The single crystal of mass $m \approx 1$ g and dimensions $6 \times 4 \times 4$ mm³ used in this study has been grown by the Czochralski technique in a tetra-arc furnace. It has been characterized by X-ray Laue. A sample from the same batch was checked by electrical resistivity, showing a residual resistivity ratio of ~ 50 and a superconducting temperature T_c of ~ 1.5 K, indicating its high quality. A slit perpendicular to the basal plane was cut into the sample to reduce the surface exposed to the pulsed field and, thus, self-heating of the sample by eddy currents.

40-T cryomagnet. A new long-duration (rising time of 23 ms and total time of > 100 ms) and high duty cycle (40, 36 and 31-T shots can be repeated every 10, 7 and 5 min, respectively) 40-T conical pulsed magnet developed by the LNCMI-Toulouse has been used. A cryostat specially designed by the ILL-Grenoble for this magnet allowed reaching temperatures down to 2 K, and the diffraction experiment was carried out on the triple-axis spectrometer IN22 (Collaborative Research Group-CEA at the ILL, Grenoble) operated in a double-axis mode with an incident neutron wavelength of 1.2 Å. At each momentum transfer, the field dependence of the neutron intensities has been extracted by summing the data accumulated over a few tens of pulsed-field shots, with either constant time- or constant field-integration windows (the rise and fall of the pulsed field were analysed separately).

Data availability. The data that support the findings of this study are available from the corresponding author on request.

References

- Mydosh, J. A. & Oppeneer, P. M. Colloquium: hidden order, superconductivity, and magnetism: the unsolved case of URu₂Si₂. *Rev. Mod. Phys.* **83**, 1301–1322 (2011).
- Palstra, T. T. M. *et al.* Superconducting and magnetic transitions in the heavy-Fermion system URu₂Si₂. *Phys. Rev. Lett.* **55**, 2727–2730 (1985).
- Vojta, M. Lattice symmetry breaking in cuprate superconductors: stripes, nematics, and superconductivity. *Adv. Phys.* **58**, 699–820 (2009).
- Fernandes, R. M., Chubukov, A. V. & Schmalian, J. What drives nematic order in iron-based superconductors? *Nat. Phys.* **10**, 97–104 (2014).
- Broholm, C. *et al.* Magnetic excitations and ordering in the heavy-electron superconductor URu₂Si₂. *Phys. Rev. Lett.* **58**, 1467–1470 (1987).
- Niklowitz, P. G. *et al.* Parasitic small-moment antiferromagnetism and nonlinear coupling of hidden order and antiferromagnetism in URu₂Si₂ observed by Larmor diffraction. *Phys. Rev. Lett.* **104**, 106406 (2010).
- Broholm, C. *et al.* Magnetic excitations in the heavy-fermion superconductor URu₂Si₂. *Phys. Rev. B* **43**, 12809–12822 (1991).
- Bourdarot, F., Raymond, S. & Regnault, L.-P. Neutron scattering studies on URu₂Si₂. *Philos. Mag.* **94**, 3702–3722 (2014).
- Ikeda, H. *et al.* Emergent rank-5 nematic order in URu₂Si₂. *Nat. Phys.* **8**, 528–533 (2012).
- Suzuki, M.-T. & Ikeda, H. Multipole order and global/site symmetry in the hidden-order phase of URu₂Si₂. *Phys. Rev. B* **90**, 184407 (2014).
- Elgazzar, S., Rusz, J., Amft, M., Oppeneer, P. M. & Mydosh, J. A. Hidden order in URu₂Si₂ originates from Fermi surface gapping induced by dynamic symmetry breaking. *Nat. Mater.* **8**, 337–341 (2009).
- Oppeneer, P. M. *et al.* Electronic structure theory of the hidden-order material URu₂Si₂. *Phys. Rev. B* **82**, 205103 (2010).
- Denlinger, J. D. *et al.* Comparative study of the electronic structure of XRu₂Si₂: probing the Anderson lattice. *J. Electron Spectrosc. Relat. Phenom.* **117–118**, 347–369 (2001).
- Janik, J. A. *et al.* Itinerant spin excitations near the hidden order transition in URu₂Si₂. *J. Phys. Condens. Matter* **21**, 192202 (2009).
- Bareille, C. *et al.* Momentum-resolved hidden-order gap reveals symmetry breaking and origin of entropy loss in URu₂Si₂. *Nat. Commun.* **5**, 4326 (2014).
- Okazaki, R. *et al.* Rotational symmetry breaking in the hidden-order phase of URu₂Si₂. *Science* **331**, 439–442 (2011).
- Tonegawa, S. *et al.* Direct observation of lattice symmetry breaking at the hidden-order transition in URu₂Si₂. *Nat. Commun.* **5**, 4188 (2013).
- Riggs, S. C. *et al.* Evidence for a nematic component to the hidden-order parameter in URu₂Si₂ from differential elastoresistance measurements. *Nat. Commun.* **6**, 6425 (2015).
- Hassinger, H. *et al.* Temperature-pressure phase diagram of URu₂Si₂ from resistivity measurements and ac calorimetry: hidden order and Fermi-surface nesting. *Phys. Rev. B* **77**, 115117 (2008).
- Bourdarot, F. *et al.* Hidden order in URu₂Si₂. *Physica B* **359361**, 986–993 (2005).
- Amitsuka, H. *et al.* Pressure–temperature phase diagram of the heavy-electron superconductor URu₂Si₂. *J. Magn. Magn. Mater.* **310**, 214–220 (2007).
- Scheerer, G. W. *et al.* Interplay of magnetism, Fermi surface reconstructions, and hidden order in the heavy-fermion material URu₂Si₂. *Phys. Rev. B* **77**, 115117 (2012).
- Kim, K. H., Harrison, N., Jaime, M., Boebinger, G. S. & Mydosh, J. A. Magnetic-field-induced quantum critical point and competing order parameters in URu₂Si₂. *Phys. Rev. Lett.* **91**, 256401 (2003).
- Aoki, D. *et al.* High-field Fermi surface properties in the low-carrier heavy-Fermion compound URu₂Si₂. *J. Phys. Soc. Jpn* **81**, 074715 (2012).
- Harrison, N. *et al.* Magnetic field-tuned localization of the 5f-electrons in URu₂Si₂. *Phys. Rev. B* **88**, 241108(R) (2014).
- Scheerer, G. W. *et al.* Fermi surface in the hidden-order state of URu₂Si₂ under intense pulsed magnetic fields up to 81 T. *Phys. Rev. B* **89**, 165107 (2014).
- Pourret, A. *et al.* Fermi surface reconstruction inside the hidden order phase of URu₂Si₂ probed by thermoelectric measurements. *J. Phys. Soc. Jpn* **2**, 034706 (2013).
- Altarawneh, M. M. *et al.* Sequential spin polarization of the Fermi surface pockets in URu₂Si₂ and its implications for the hidden order. *Phys. Rev. Lett.* **106**, 146403 (2011).
- Pourret, A. *et al.* Quantum criticality and Lifshitz transition in the Ising system CeRu₂Si₂: comparison with YbRu₂Si₂. *J. Phys. Soc. Jpn* **83**, 061002 (2014).
- Yokoyama, M. *et al.* Neutron scattering study on competition between hidden order and antiferromagnetism in U(Ru_{1-x}Rh_x)₂Si₂ ($x \leq 0.05$). *J. Phys. Soc. Jpn* **73**, 545–548 (2004).
- Oh, Y. S., Kim, K. H., Harrison, N., Amitsuka, H. & Mydosh, J. A. Decrease of the coherence temperature with low Rh doping in U(Ru_{1-x}Rh_x)₂Si₂. *J. Magn. Magn. Mater.* **310**, 855–857 (2007).
- Kim, K. H. *et al.* Nexus between quantum criticality and phase formation in U(Ru_{1-x}Rh_x)₂Si₂. *Phys. Rev. Lett.* **93**, 206402 (2004).

33. Kuwahara, K. *et al.* Magnetic structure of phase II in $U(\text{Ru}_{0.96}\text{Rb}_{0.04})_2\text{Si}_2$ determined by neutron diffraction under pulsed high magnetic fields. *Phys. Rev. Lett.* **110**, 216406 (2013).
34. Scheerer, G. W., Knafo, W., Aoki, D. & Flouquet, J. Angular dependence of the high-magnetic-field phase diagram of URu_2Si_2 . *J. Phys. Soc. Jpn* **81**, SB005 (2012).
35. Fawcett, E. Spin-density-wave antiferromagnetism in chromium. *Rev. Mod. Phys.* **60**, 209–283 (1988).
36. Kenzelmann *et al.* Coupled superconducting and magnetic order in CeCoIn_5 . *Science* **321**, 1652–1654 (2008).
37. Lester, C. S. *et al.* Field-tunable spin-density-wave phases in $\text{Sr}_3\text{Ru}_2\text{O}_7$. *Nat. Mater.* **14**, 373–378 (2015).
38. Sakai, H. *et al.* Emergent antiferromagnetism out of the “hidden-order” state in URu_2Si_2 : high magnetic field nuclear magnetic resonance to 40 T. *Phys. Rev. Lett.* **112**, 236401 (2014).
39. Aphi, T., Mikac, U., Seliger, J., Dolinšek, J. & Blinc, R. Evidence for a $1 - q$ to $3 - q$ transition and $3 - q$ soliton lattice in incommensurate proustite. *Phys. Rev. Lett.* **80**, 2225–2228 (1998).
40. Kuwahara, K. *et al.* Magnetic form factor of URu_2Si_2 . *Physica B* **378–380**, 581–582 (2006).
41. White, R. M. *Quantum Theory of magnetism* (Springer, 2007).
42. LeR., Dawson, A., Datars, W. R., Garrett, J. D. & Razavi, F. S. Electrical transport in URu_2Si_2 . *J. Phys. Condens. Matter* **1**, 6817–6828 (1989).
43. Kasahara, Y. *et al.* Exotic superconducting properties in the electron-hole-compensated heavy-fermion ‘semimetal’ URu_2Si_2 . *Phys. Rev. Lett.* **99**, 116402 (2007).
44. Bel, R., Jin, H., Behnia, K., Flouquet, J. & Lejay, P. Thermoelectricity of URu_2Si_2 : Giant Nernst effect in the hidden-order state. *Phys. Rev. B* **70**, 220501 (2004).
45. Santander-Syro, A. F. *et al.* Fermi-surface instability at the ‘hidden-order’ transition of URu_2Si_2 . *Nat. Phys* **5**, 637–641 (2009).
46. Niklowitz, P. G. *et al.* Role of commensurate and incommensurate low-energy excitations in the paramagnetic to hidden-order transition of URu_2Si_2 . *Phys. Rev. B* **92**, 115116 (2015).
47. Aoki, D., Knafo, W. & Sheikin, I. Heavy fermions in a high magnetic field. *C. R. Physique* **14**, 53–77 (2013).
48. Villaume, A. *et al.* Signature of hidden order in heavy fermion superconductor URu_2Si_2 : resonance at the wave vector $\mathbf{Q}_0 = (1,0,0)$. *Phys. Rev. B* **78**, 012504 (2008).
49. Aoki, D. *et al.* Field reentrance of the hidden order state of URu_2Si_2 under pressure. *J. Phys. Soc. Jpn* **78**, 053701 (2009).
50. Pfleiderer, C., Mydosh, J. A. & Vojta, M. Pressure dependence of the magnetization of URu_2Si_2 . *Phys. Rev. B* **74**, 104412 (2006).
51. Bourdarot, F., Fåk, B., Habicht, K. & Prokeš, K. Inflection point in the magnetic field dependence of the ordered moment of URu_2Si_2 observed by neutron scattering in fields up to 17 T. *Phys. Rev. Lett.* **90**, 067203 (2003).
52. Sato, M. *et al.* Field-induced ferromagnetic correlation in the metamagnetic crossover in CeRu_2Si_2 as studied by neutron scattering. *J. Phys. Soc. Jpn* **73**, 3418–3421 (2004).
53. Knafo, W., Raymond, S., Lejay, P. & Flouquet, J. Antiferromagnetic criticality at a heavy-fermion quantum phase transition. *Nat. Phys.* **5**, 753–757 (2009).
54. Dixon, I. R. *et al.* Final assembly of the Helmholtz-Zentrum Berlin Series-connected hybrid magnet system. *IEEE Trans. Appl. Supercond.* **25**, 4300204 (2015).
55. Oh, Y. S. *et al.* Interplay between Fermi surface topology and ordering in URu_2Si_2 revealed through abrupt Hall coefficient changes in strong magnetic fields. *Phys. Rev. Lett.* **98**, 016401 (2007).

Acknowledgements

We acknowledge R. Ballou, J. Béard, P. Dalmas de Réotier, H. Ikeda, M.-H. Julien, M. Horvatic, E. Ressouche and G Rikken for useful discussions. Part of this work was funded by the ANR grant Magfins N° ANR-10-0431. H.N. acknowledges KAKENHI 23224009. D.A. acknowledges KAKENHI, 15H05745, 15H05882, 15H05884, 15K21732, 25247055. H.N. and D.A. acknowledge support by ICC-IMR.

Author contributions

All co-authors conceived this project. D.A. has grown, characterized and prepared the single crystal studied here. J.B. and P.F. designed and developed the pulsed-field magnet. X.T. and E.L.-B. designed and developed a special cryostat for this magnet. W.K., F.D., F.B., K.K., H.N. and L.-P.R. performed the neutron scattering experiment. W.K. and F.D. analysed the data. W.K., F.D., F.B., J.F. and L.-P.R. wrote the paper, with inputs from the other co-authors.

Additional information

Supplementary Information accompanies this paper at <http://www.nature.com/naturecommunications>

Competing financial interests: The authors declare no competing financial interests.

Reprints and permission information is available online at <http://npg.nature.com/reprintsandpermissions/>

How to cite this article: Knafo, W. *et al.* Field-induced spin-density wave beyond hidden order in URu_2Si_2 . *Nat. Commun.* **7**, 13075 doi: 10.1038/ncomms13075 (2016).



This work is licensed under a Creative Commons Attribution 4.0 International License. The images or other third party material in this article are included in the article’s Creative Commons license, unless indicated otherwise in the credit line; if the material is not included under the Creative Commons license, users will need to obtain permission from the license holder to reproduce the material. To view a copy of this license, visit <http://creativecommons.org/licenses/by/4.0/>

© The Author(s) 2016